The Journal of Experimental Biology 205, 2737–2744 (2002)
Printed in Great Britain © The Company of Biologists Limited 2002
JEB4180

Fluid-dynamic characteristics of a bristled wing

S. Sunada[1,*], H. Takashima[2], T. Hattori[2], K. Yasuda[2] and K. Kawachi[3]

[1]*National Institute of Industrial Science and Technology, Ministry of Economy, Trade and Industry, 1-2-1 Namiki, Ibaraki 305-8964, Japan,* [2]*Nihon University, 7-24-1 Narashinodai, Funabashi, Chiba 274-0081, Japan* and [3]*Research Center for Advanced Science and Technology, University of Tokyo, 4-6-1 Komaba, Meguro, Tokyo 153-8904, Japan*

*Author for correspondence at present address: Osaka Prefecture University, 1-1 Gakuen-cho, Sakai, Osaka 599-8531, Japan (e-mail: sunada@aero.osakafu-u.ac.jp)

Accepted 6 June 2002

Summary

Thrips fly at a chord-based Reynolds number of approximately 10 using bristled rather than solid wings. We tested two dynamically scaled mechanical models of a thrips forewing. In the bristled design, cylindrical rods model the bristles of the forewing; the solid design was identical to the bristled one in shape, but the spaces between the 'bristles' were filled in by membrane. We studied four different motion patterns: (i) forward motion at a constant forward velocity, (ii) forward motion at a translational acceleration, (iii) rotational motion at a constant angular velocity and (iv) rotational motion at an angular acceleration. Fluid-dynamic forces acting on the bristled model wing were a little smaller than those on the solid wing. Therefore, the bristled wing of a thrips cannnot be explained in terms of increased fluid-dynamic forces.

Key words: thrips, *Thripidae frankliniella*, bristled wing, membranous wing, fluid-dynamics, constant-velocity translation/rotation, accelerating translation/rotation.

Introduction

Numerous animals use hairy appendages for feeding and locomotion. Extensive research has been carried out on the flow volume through the hairs on feeding appendages (e.g. Koehl, 1983, 1995; Hansen and Tiselius, 1992), but there is not much information on the fluid-dynamic forces generated by hairy appendages (Horridge, 1956; Ellington, 1980; Cheer and Koehl, 1987; Kuethe, 1975; Tanaka, 1995). How to estimate the fluid-dynamic forces acting on the hairy appendages at low and very low Reynolds number has not therefore been clarified.

To estimate the fluid-dynamic forces acting on the hairy appendages and understand the fluid-dynamic mechanisms of thrips flight, we measured the fluid-dynamic characteristics of a dynamically scaled model of the forewing. Four different wing motions were studied: forward motion at a constant velocity (constant-velocity translation), forward motion at a translational acceleration (accelerating translation), rotational motion at a constant angular velocity (constant-velocity rotation) and rotational motion at an angular acceleration (accelerating rotation). For comparison, the fluid-dynamic characteristics of a solid model wing were also measured. The solid wing had the same outline as the bristled model, but was made from a solid flat plate of the same thickness as the bristle diameter. Comparing the fluid-dynamic performance of the bristled and the solid wing might help to clarify why a small insect, such as a thrips, uses bristled wings for flight.

Materials and methods

Wing shape

The fore- and hindwings of a real thrips *Thripidae frankliniella* intonsa) are shown in Fig. 1A. Fig. 1B,C shows diagrams of the bristled wing and solid model wings, respectively. The bristled wing comprises a membrane and 51 cylinders. Table 1 lists the dimensions of a thrips' forewing, measured by Tanaka (1995), and of the model wings, where x_w is wing length, c is chord length, c_m is membrane width, d is cylinder diameter, c_{h1} is the length of cylinders on the leading edge of the membrane, c_{h2} is the length of cylinders on the trailing edge of the membrane, n is the number of cylinders on each edges, D is the distance between neighbouring cylinders, and S is the wing surface area. S for the bristled wing is the sum of the cylinder frontal area $nd(c_{h1}+c_{h2})$ and the membrane area $x_w c_m$. The solid wing has a surface area $x_w c$. The parameters x_w/c, c_m/c, d/x_w, c_{h1}/c, c_{h2}/c, n and D/d are similar for both the bristled wing and a real thrips' forewing, maintaining geometric scaling. The fluid-dynamic characteristics of the bristled wing and the solid wing were measured for four motion patterns.

Forward motion

Fig. 2 shows the apparatus used to measure the fluid-dynamic forces acting on the model wings in forward motion. A tank (dimensions in X, Y and Z directions, L_X=800 mm, L_Y=400 mm and L_Z =500 mm, respectively) was filled with an

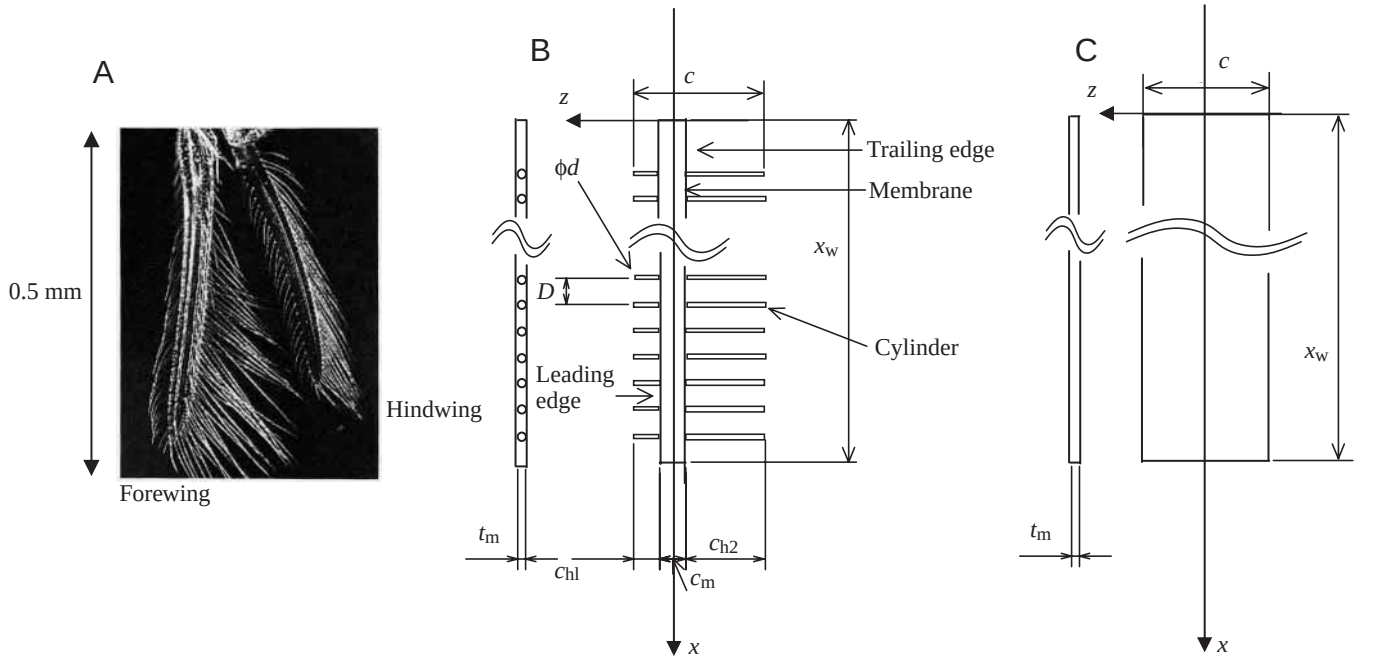

Fig. 1. Test wings. (A) Photomicrograph of a thrip's wings. (B,C) Diagrams of a bristled model wing (B) and a solid model wing (C). *c*, chord length of a wing; c_m, membrane width of a bristled wing; c_{h1}, length of cylinders on the leading edge; c_{h2}, length of cylinders on the trailing edge; *D*, distance between neighbouring cylinders or bristles; *d*, diameter of cylinders or bristles; t_m, thickness of a wing; x_w, wing length; *x*,*y*,*z*, wing-fixed coordinate system.

aqueous solution of glycerine. The wing was suspended from a load cell (LMC3729-1N, Nissho Electric Works, Japan) *via* an 8 mm diameter joint cylinder. The load cell can measure forces in the *x* and *z* directions, F_x and F_z, and the moment around the *y* axis, M_y. The maximum load for F_x and F_z was 1 N and that for M_y was 0.01 N m.

The cross talk between F_x, F_z and M_y was small, and the measured forces F_x and F_z were considered to be equal to the normal and tangential forces, F_n and F_t, respectively, on the wing (F_x=F_n, F_z=–F_t).

The wing was moved in the *X* direction at a constant angle of attack α between –10 ° and 45 ° as described for constant-velocity translation and accelerating translation in Table 2. During constant-velocity translation, the wing moved at a constant forward velocityV_0. During accelerating translation, the wing underwent sinusoidal acceleration for $t \leq T_{0t}$ ($t \leq T_{0t}$ =4 or 10 s), where *t* is time and T_{0t} is the period of accelerated motion. The forward velocity reached a terminal value V_0 at $t = T_{0t}$. Because the tank was much larger than the model wings, wall and surface effects can be ignored.

Table 2 also shows the Reynolds number *Re* calculated as follows:

$$Re = V_0 c/\nu\,, \qquad (1)$$

where ν is the kinematic viscosity of the liquid. During constant-velocity translation and accelerating translation, *Re*=12, which is similar to the *Re*=10 for a flying thrips (Tanaka, 1995).

The fluid-dynamic forces acting on the wing were measured as follows. First, the normal and tangential forces $F_{n,c}$ and $F_{t,c}$ were measured for the wing mount only without the wing connected to the joint cylinder. Next, we measured the normal and tangential forces F_n and F_t generated by both the wing and its mount. The fluid-dynamic forces acting on the wing only were calculated from the measured forces, F_n, F_t, $F_{n,c}$ and $F_{t,c}$ for the two translational motions.

Table 1. *Size of model wings and thrips' wing*

Wing	*c* (mm)	x_w/c	d/c	c_m/c	c_{h1}/c	c_{h2}/c	t_m/c	*S* (mm^2)	D/d	*n*
Thrips*	3×10^{-1}	2.7	5×10^{-3}	2×10^{-1}	1.3×10^{-1}	6.7×10^{-1}	–	6×10^{-2}	10	50
Bristled model	60	3.0	5×10^{-3}	2×10^{-1}	1.8×10^{-1}	6.2×10^{-1}	10^{-2}	2.9×10^{3}	10	51
Solid model	60	3.0	–	–	–	–	10^{-2}	1.1×10^{4}	–	–

*Data for the thrips' wing were obtained by Tanaka (1995).

c, chord length; x_w, wing length; *d*, diameter of bristles or cylinders; c_m, membrane width; c_{h1}, length of bristles or cylinders on the leading edge; c_{h2}, length of bristles or cylinders on the trailing edge; t_m, thickness of the wing; *S*, wing surface area; *D*, distance between neighbouring bristles or cylinders; *n*, the number of bristles or cylinders.

Constant-velocity translation

The forces F_n, F_t, $F_{n,c}$ and $F_{t,c}$ were measured when they reached constant values. The fluid-dynamic forces acting on the wing only were calculated using the expressions, F_n–$F_{n,c}$ and F_t–$F_{t,c}$. The lift coefficient C_L and drag coefficient C_D were obtained by non-dimensionalizing the measured fluid-dynamic forces as follows:

$$C_L = [(F_n - F_{n,c})\cos\alpha - (F_t - F_{t,c})\sin\alpha]/0.5\rho V_0^2 S, \quad (2)$$

$$C_D = [(F_n - F_{n,c})\sin\alpha + (F_t - F_{t,c})\cos\alpha]/0.5\rho V_0^2 S. \quad (3)$$

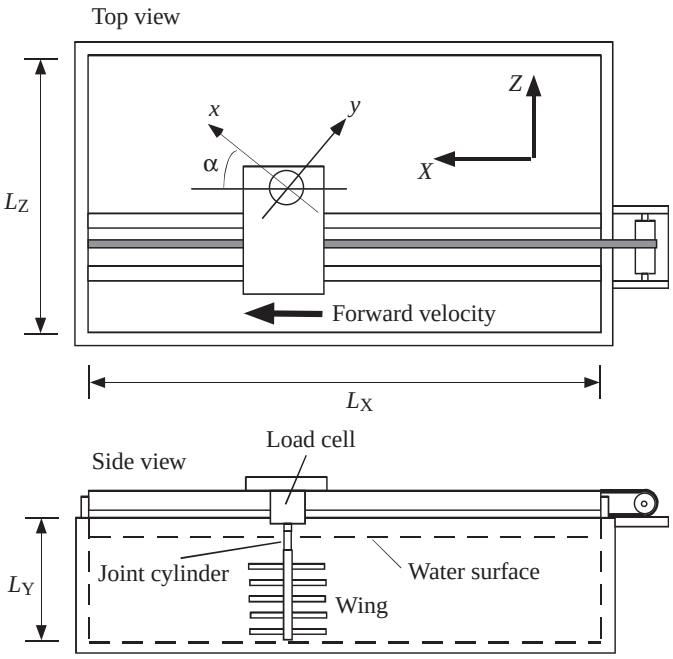

Fig. 2. Experimental apparatus used to measure the fluid-dynamic forces of a wing in forward motion (constant-velocity translation and accelerating translation). *X*, *Y*, *Z*, earth-fixed coorinate system; *x*, *y*, *z*, wing-fixed coordinate system; L_X, L_Y, L_Z, dimensions of the tank; α, angle of attack.

Accelerating translation

The forces F_n, F_t, $F_{n,c}$ and $F_{t,c}$ were measured at $0 \leq t \leq T_{0t}$. F_n and F_t are the sum of the fluid-dynamic and inertial forces acting on the joint cylinder, the fluid-dynamic and inertial forces acting on the wing and the inertial forces on the load cell. $F_{n,c}$ and $F_{t,c}$ are the sum of the fluid-dynamic and inertial forces acting on the joint cylinder and the inertial forces acting on the load cell. The load cell measured an inertial force proportional to the accelerated mass attached to the strain gauge in the load cell. Therefore, F_n–$F_{n,c}$ and F_t–$F_{t,c}$ are the sum of the fluid-dynamic and inertial forces acting on the wing. The normal and tangential fluid-dynamic forces acting only on the wing are given by F_n–$F_{n,c}$–$m_w\ddot{X}\sin\alpha$ and F_t–$F_{t,c}$–$m_w\ddot{X}\cos\alpha$, respectively, where m_w is the mass of the wing, and $m_w\ddot{X}\sin\alpha$ and $m_w\ddot{X}\cos\alpha$ are the normal and tangential components, respectively, of the inertial force acting on the wing. C_L and C_D were obtained by non-dimensionalizing the measured fluid-dynamic forces as follows:

$$C_L = [(F_n - F_{n,c})\cos\alpha - (F_t - F_{t,c})\sin\alpha]/0.5\rho \dot{X}^2 S, \quad (4)$$

$$C_D = [(F_n - F_{n,c})\sin\alpha + (F_t - F_{t,c})\cos\alpha - m_w\ddot{X}]/0.5\rho \dot{X}^2 S. \quad (5)$$

Rotational motion

Fig. 3 shows the apparatus used to measure the fluid-dynamic forces acting on the model wings in rotational

Table 2. *Wing motions*

Motion pattern	Wing motions	Non-dimensional values
Constant-velocity translation	Displacement $X=V_0t$, $V_0=2.4\times10^{-2}$ m s^{-1}	Reynolds number $Re=\frac{V_0c}{\nu}=12$
Accelerating translation	Displacement $X=\frac{V_0}{2}\left(t-\frac{T_{0t}}{\pi}\sin\frac{t}{T_{0t}}\pi\right)$, $0\leq t\leq T_{0t}$	Reynolds number $Re=\frac{V_0c}{\nu}=12$
	$V_0=2.4\times10^{-2}$ m s^{-1}, $T_{0t}=4$, 10 s	Non-dimensional total displacement $\frac{V_0T_{0t}}{2c}=0.8$ ($T_{0t}=4$ s), $\frac{V_0T_{0t}}{2c}=2$ ($T_{0t}=10$ s)
Constant-velocity rotation	Rotational angle $\phi=\omega t$, $\omega=0.2$ rad s^{-1}	Reynolds number $Re=\frac{\left(\frac{3}{4}x_W\right)\omega c}{\nu}=10$
Accelerating rotation	Rotational angle $\phi=\frac{\Phi}{2}\left(1-\cos\left(\frac{t}{T_{0r}}\frac{\pi}{2}\right)\right)$,	Reynolds number $Re=\frac{\left(\frac{3}{4}x_W\right)\left(\frac{\pi}{2\sqrt{2}T_{0r}}\right)\frac{\Phi}{2}c}{\nu}=9.6$
	$0\leq t\leq T_{0r}$, $\Phi=2.3$ rad, $T_{0r}=6.5$ s	Amplitude of accelerating rotation $\frac{\Phi}{2}=1.15$ rad

V_0, terminal forward velocity; t, time; T_{0t}, period of accelerated phase in translational motion; ω, angular velocity for constant-velocity rotation; Φ/2, amplitude of accelerating rotation; T_{0r}, period of accelerated phase in rotational motion; c, chord length; ν, kinematic viscosity; x_w, wing length.

motion. The model wing was suspended in a tank (L_X, L_Y=500 mm and L_Z=1000 mm) filled with an aqueous solution of glycerine. The wing was mounted onto a load cell (LMC2909, Nissho Electric Works, Japan) and a motor *via* a 6 mm diameter joint cylinder. The wing rotated around the joint cylinder in the *X*–*Y* plane. The load cell measured force in the *Z* direction, F_z, and the moment around the *Z* axis, M_z. The maximum load was 5 N for F_z and 0.25 N m for M_z. When forces in the *X*, *Y* and *Z* directions and moments around the *X*, *Y* and *Z* axes act on the load cell, the output signal from the load cell, F_z and M_z are affected by all the forces and moments acting on the load cell. However, because the cross talk between F_z and M_z was small, measured values of F_z and M_z were considered to be equal to the force in the *Z* direction and the moment around the *Z* axis actually acting on the load cell, respectively.

The tank was filled to the depth L_{Z1} of 980 mm with an aqueous solution of glycerine. The rotational axis of the wing was at the centre of the tank in the *X*–*Y* plane. The distance between the rotational plane and the bottom of the tank was $0.7L_{Z1}$. All tank dimensions are large enough for surface and wall effects to be negligible.

The geometrical angle of attack α was defined as the angle between the *Z* axis and a vector normal to the wing. The angle of attack α was set between –10 ° and 45 °.

Table 2 lists the rotational angle ϕ during constant-velocity rotation and accelerating rotation and lists *Re* defined for constant-velocity rotation as

$$Re = \frac{(3/4x_w)\omega c}{\nu}, \tag{6}$$

and for accelerating rotation,

$$Re = \frac{(3/4x_w)(\pi/2\sqrt{2}T_{0r})(\Phi/2)c}{\nu}, \tag{7}$$

where ω is the rotational angular velocity for constant-velocity rotation, T_{0r} and $\Phi/2$ are the period and amplitude, respectively, of accelerating rotation, and $(\pi/2\sqrt{2}T_{0r})(\Phi/2)$ is the averaged angular velocity. For constant-velocity rotation and accelerating rotation, *Re* was approximately 10, which is close to the *Re* for a flying thrips (Tanaka, 1995).

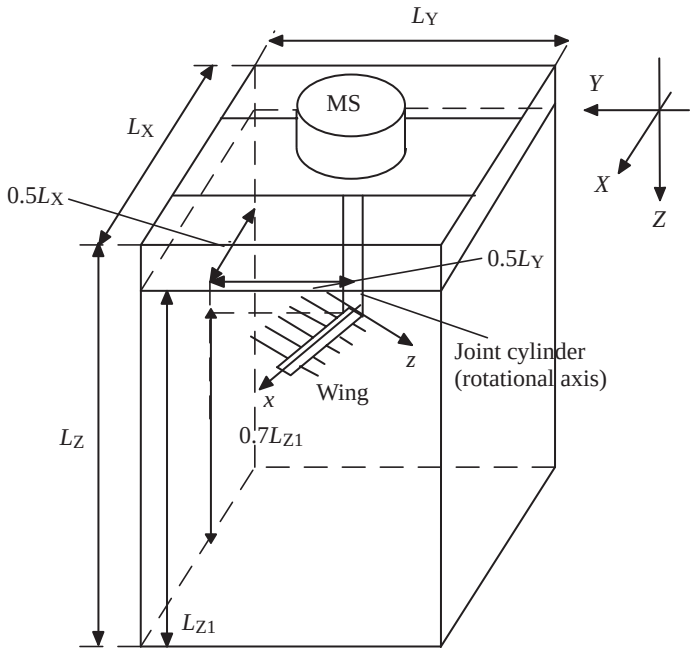

Fig. 3. Experimental apparatus used to measure the fluid-dynamic forces of a wing in rotational motion (constant-velocity rotation and accelerating rotation). The measuring system (MS) comprises a load cell and a motor. *X*, *Y*, *Z*, earth-fixed coordinate system; *x*, *y*, *z*, wing-fixed coordinate system; L_X, L_Y, L_Z, dimensions of the tank; L_{Z1}, depth of liquid; $0.5L_X$, $0.5L_Y$, $0.5L_Z$, position of a root of a wing.

Constant-velocity rotation

We measured the force in the –*Z* direction, i.e. thrust *T*, and the moment around the *Z* axis, i.e. torque *Q*, after the wing had completed 30 rotations. The measured *T* and *Q* were considered to be equal to the fluid-dynamic thrust and torque of the wing because the forces acting on the joint cylinder were much smaller than those acting on the wing. C_L and C_D were determined by non-dimensionalizing the measured fluid-dynamic thrust and torque as follows (Ellington, 1984):

$$C_L = T/0.5\rho \int_0^{x_w} (x\omega)^2 c(x)\mathrm{d}x, \tag{8}$$

$$C_D = Q/0.5\rho \int_0^{x_w} (x\omega)^2 xc(x)\mathrm{d}x. \tag{9}$$

where *x* is span-wise axis, shown in Fig. 1.

Accelerating rotation

Thrust *T* and torque *Q* were measured for $0 \le t \le T_{0r}$ in an aqueous solution of glycerine. As in the case of constant-velocity rotation, we neglected the forces acting on the joint cylinder and assumed that the measured thrust *T* is equal to the fluid-dynamic thrust. The measured torque is the sum of the fluid-dynamic torque acting on both the wing and the joint cylinder, as well as the inertial torque acting on the wing, on the joint cylinder and on the load cell. Because the fluid-dynamic torque acting on the joint cylinder is much smaller than that acting on the wing, the former torque can be neglected. We measured the torque in air to estimate the inertial torque acting on the wing, on the joint cylinder and on the load cell. The measured torque in air, Q_c, was approximately equal to the inertial torque acting on the wing, on the joint cylinder and on the load cell because their density is much larger than the density of air and, hence, the fluid-dynamic torque in air was much smaller than the inertial torque acting on these three components (wing, joint cylinder and load cell). Therefore, the fluid-dynamic torque acting on the wing was obtained from Q–Q_c.

C_L and C_D were determined by non-dimensionalizing the measured fluid-dynamic thrust and torque as follows (Ellington, 1984):

$$C_L = T/0.5\rho \int_0^{x_w} (x\dot{\phi})^2 c(x)\mathrm{d}x\,, \quad (10)$$

and

$$C_D = (Q - Q_c)/0.5\rho \int_0^{x_w} (x\dot{\phi})^2 x c(x)\mathrm{d}x\,, \quad (11)$$

where $\dot{\phi}$ is the instantaneous angular velocity.

Results

Fig. 4 compares the fluid-dynamic forces for the steady motions, constant-velocity translation and constant-velocity rotation, and shows the ratio of lift L acting on the bristled wing to that acting on the solid wing and the ratio of drag D acting on the bristled wing to that acting on the solid wing for constant-velocity translation. Also shown is the ratio of thrust T acting on the bristled wing to that acting on the solid wing and the ratio of torque Q acting on the bristled wing to that acting on the solid wing, for constant-velocity rotation. The ratios of lift, drag, thrust and torque acting on the bristled wing to those on the solid wing were a little less than 1, except for constant-velocity rotation (T; at α=10 ° and 20 °). During steady motion (constant-velocity translation and constant-velocity rotation), the fluid-dynamic forces acting on the bristled wing were smaller than those acting on the solid wing, except for constant-velocity rotation (T; at α=10 ° and 20 °).

Fig. 5 shows C_L and C_D plotted *versus* α for constant-velocity translation and constant-velocity rotation. For both motions, C_L and C_D of the bristled wing were larger than those of the solid wing. The differences in C_L and C_D between constant-velocity rotation and constant-velocity translation for the bristled wing are larger than those for the solid wing. Hence, the flow around the bristled wing should exhibit large differences between constant-velocity rotation and constant-velocity translation than the solid wing. Fig. 6 shows how lift and drag change with distance travelled for the solid wing

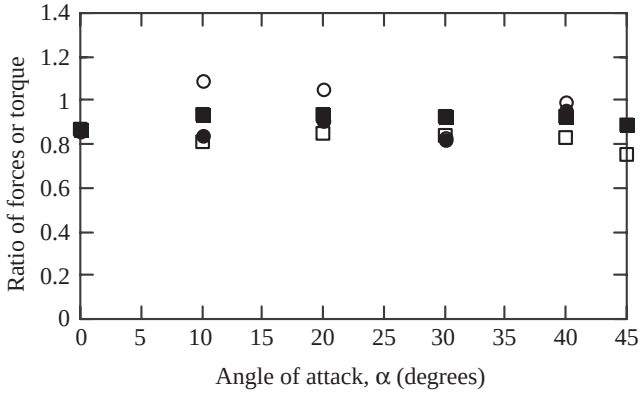

Fig. 4. Ratio of forces (lift L, drag D in constant-velocity translation and thrust T in constant-velocity rotation) or torque (Q in constant-velocity rotation) acting on the bristled wing to those on the solid wing. Open squares, L, filled squares, D, in constant-velocity translation; open circles, T, filled circles, Q, in constant-velocity rotation.

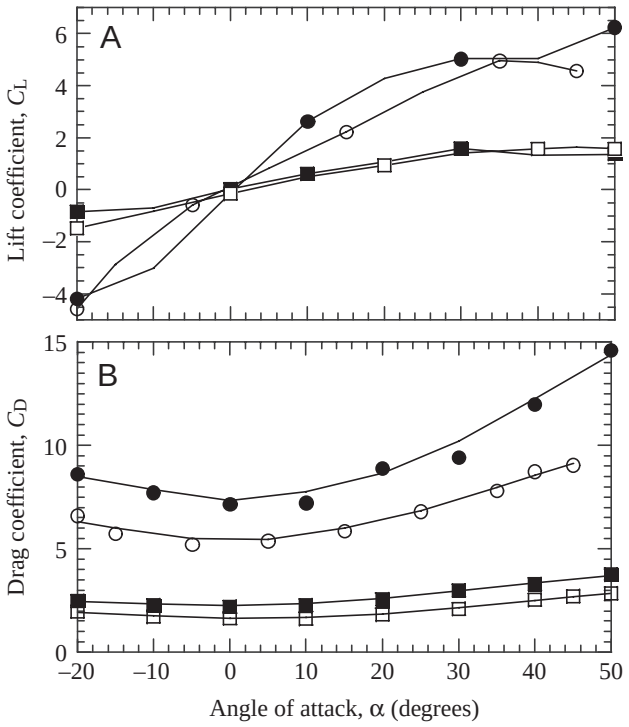

Fig. 5. Lift coefficient C_L (A) and drag coefficient C_D (B) for steady motion (constant-velocity translation and constant-velocity rotation). Open circles, the bristled wing in constant-velocity translation; filled circles, the bristled wing in constant-velocity rotation; open squares, the solid wing in constant-velocity translation; filled squares, the solid wing in constant-velocity rotation.

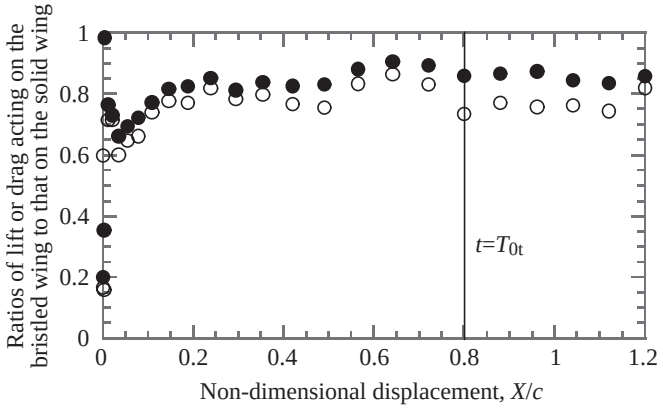

Fig. 6. Ratios of lift (open circles) and drag (filled circles) acting on the bristled wing in accelerating translation (T_{0t}=4 s and α=45 °) to those on the solid wing. t, time (s); T_{0t}, period of acceleration phase in translational motion; α, angle of attack.

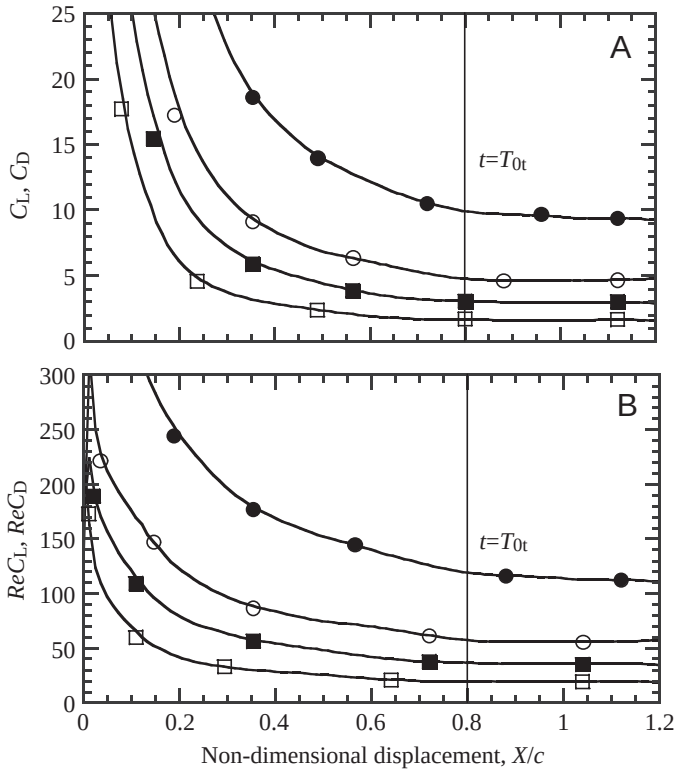

Fig. 7. Changes in time of C_L and C_D (A) and those of ReC_L and ReC_D (B) for accelerating translation, when T_{0t}=4 s and α=45 °. t, time (s); T_{0t}, period of acceleration phase in translational motion; α, angle of attack. Open circles, C_L or ReC_L for the bristled wing; filled circles, C_D or ReC_D for the bristled wing; open squares, C_L or ReC_L for the solid wing; filled squares, C_D or ReC_D for the solid wing.

during accelerating translation (α=45 ° and T_{0t}=4 s). The lift-to-drag ratio was between 0.8 and 1. During this unsteady translation, the fluid-dynamic forces acting on the bristled wing were smaller than those acting on the solid wing. Fig. 7A shows how C_L and C_D vary with distance travelled for accelerating translation when α=45 ° and T_{0t}=4 s. When $t=T_{0t}$, the non-dimensional displacement X/c was approximately 0.8. The figure shows that neither C_L nor C_D reached a constant value when $t=T_{0t}$ and that the forward velocity $\dot{X}$ reached its terminal value V_0. Furthermore, C_L and C_D were larger for $t\leq T_{0t}$ than at $t=T_{0t}$. Fluid-dynamic forces due to added mass (Ellington, 1984), which act on the wings when $t<T_{0t}$, are negligible. The larger values of C_L and C_D for $t\leq T_{0t}$ might be explained in two ways. First, Re defined by instantaneous forward velocity $\dot{X}$ was smaller for $t<T_{0t}$ than at $t=T_{0t}$. For $Re<10^3$, C_L and C_D, which are non-dimensionalized by $\dot{X}^2$, increase as Re decreases. For $Re<1$, C_L and C_D are proportional to $1/Re$ and ReC_L and ReC_D are independent of Re (e.g. Hoerner, 1965). Second, wing motion accelerated while $t\leq T_{0t}$, and this acceleration caused an increase in C_L and C_D. This increase is expected to be caused by 'delayed stall' (Dickinson et al., 1999).

To test the first hypothesis, we looked at how ReC_L and ReC_D changed over time for accelerating translation when

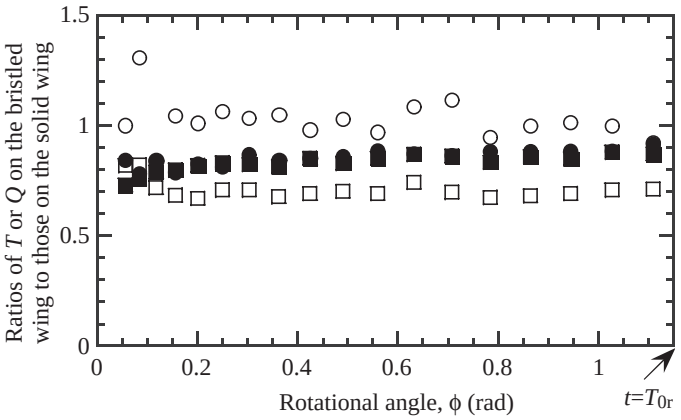

Fig. 8. Ratios of thrust T and torque Q acting on the bristled wing in accelerating rotation (α=20 ° and α=45 °) to those on the solid wing. t, time (s); T_{0r}, period of acceleration phase in rotational motion; α, angle of attack. Open circles, T at α=20 °; filled circles, Q at α=20 °; open squares, T at α=45 °; filled squares, Q at α=45 °.

α=45 ° and T_{0t}=4 s (Fig. 7B). These changes over time were smaller than those of C_L and C_D shown in Fig. 7A. However, ReC_L and ReC_D were larger for $t<T_{0t}$ than at $t=T_{0t}$. Therefore, the second hypothesis is also needed to explain the differences in C_L and C_D for $t<T_{0t}$ than at $t=T_{0t}$. This might apply not just for T_{0t}=4 s but also for T_{0t}=10 s.

Fig. 8 shows the changes over time of the ratios of thrust T and torque Q acting on the bristled wing to those acting on the solid wing for accelerating rotation for α=20 ° and 45 °. These ratios were less than 1, except for the ratio at α=20 °, when the fluid-dynamic forces acting on the bristled wing were larger than those acting on the solid wing.

Fig. 9A shows changes over time of C_L and C_D for accelerating rotation when α=45 °. The coefficients C_L and C_D of the solid wing were smaller than those of the bristled wing. The C_L and C_D for $t<T_{0r}$ were larger than those at $t=T_{0r}$. The fluid-dynamic forces due to added mass (Ellington, 1984) are negligible while $t<T_{0r}$. The changes over time of ReC_L and ReC_D in Fig. 9B show the differences in C_L and C_D for $t<T_{0r}$ and $t=T_{0r}$. Just as during accelerating translation, ReC_L and ReC_D are larger for $t<T_{0r}$, and again this difference is due to delayed stall.

Discussion

Fluid-dynamic forces acting on the geometrically scaled bristled model wing were smaller than those acting on the solid wing. With a few exceptions, this result was valid for all the four wing motions: (i) forward motion at a constant forward velocity, (ii) forward motion at a translational acceleration, (iii) rotational motion at a constant angular velocity and (iv) rotational motion at an angular acceleration. The bristled wings of a thrips cannot therefore be explained by an augumentation of fluid-dynamic performance.

Fig. 10A shows the relationship between mass m and wing-beat frequency f for a thrips (Tanaka, 1995) and a variety of

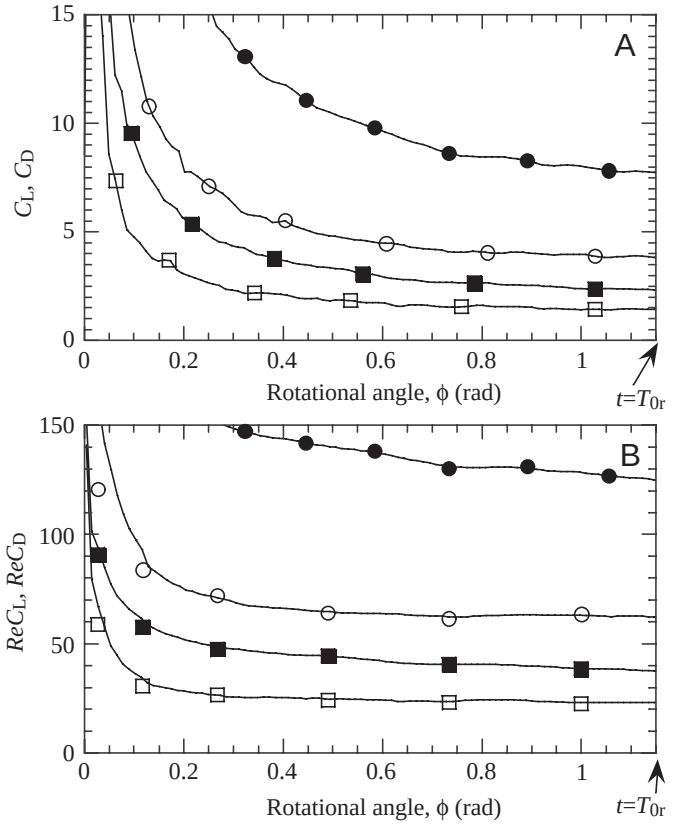

Fig. 9. Changes in time of C_L and C_D (A) and ReC_L and ReC_D (B) for accelerating rotation, when α=45°. *t*, time (s); T_{0r}, period of accelerated phase in rotational motion; α, angle of attack. Open circles, C_L or ReC_L for the bristled wing; filled circles, C_D or ReC_D for the bristled wing; open squares, C_L or ReC_L for the solid wing; filled squares, C_D or ReC_D for the solid wing.

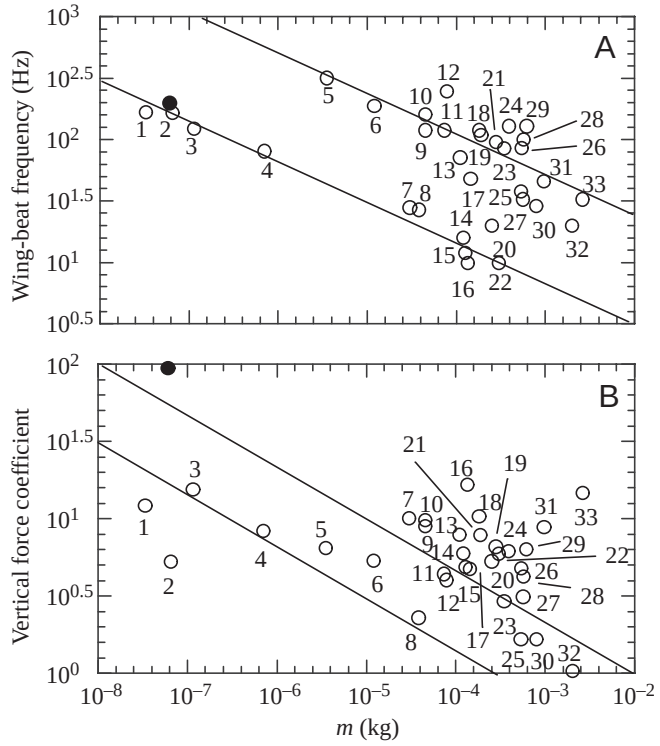

Fig. 10. Comparison of flight data for a thrip and for other insects. (A) mass (kg) *m versus* wing-beat frequency (Hz) *f*, (B) mass (kg) *m versus* a parameter indicating vertical force coefficient $m\boldsymbol{g}/S_{tot}(x_w f)^2$. Data for the thrips (filled circle) are from Tanaka (1995). Data for the following insects (open circles) are from Azuma (1992): [1]*Bemisia tabaci*, [2]*Aleurothrixus floccosus*, [3]*Aphis gossypii*, [4]*Acyrthosiphon kondoi*, [5]*Aedes nearcticus*, [6]*Musca domestica*, [7]*Panorpa communis* L., [8]*Pyrosoma minimum* Harr., [9]*Amonophila sabulosa* V.del, [10]*Sarcophaga carnaria* L., [11]*Volucella pellucens* Meig., [12]*Apis mellifica* L., [13]*Telepharus fuscus*, [14]*Calopteryx splendes* Harr., [15]*Pieris brassica* L., [16]*Vanessa atolanta* L., [17]*Plusia gamma* L., [18]*Talanus affioris*, [19]*Vespa germanica*, [20]*Orthetrum caerulescens* Fabr., [21]*Tabanus botinus*, [22]*Papilio podalirius*, [23]*Macroglossa stellatorum* L., [24]*Bombus terrestris* Fabr., [25]*Aeschna mixtra* Latr., [26]*Cetonia aurata*, [27]*Brachytron pratense* Mull., [28]*Vespa crabro* L., [29]*Xylocope violacea*, [30]*Anax parthenope*, [31]*Melolontha vulgaris* Fabr., [32]*Schistocerca gregaria*, [33]*Lucanus corcus*.

other insects (Azuma, 1992). The wing-beat frequency *f* of the thrips is 200 Hz, which is relatively low for its body mass ($m \approx 6\times10^{-8}$ kg) compared with larger insects, but similar to that of other small insects, such as *Bemisia tabaci*, *Aleurothrixus floccosus*, *Aphis gossypii* and *Acyrthosiphon kondoi* (numbered 1–4 in Fig. 10A, respectively). Fig. 10B shows the values of $m\boldsymbol{g}/S_{tot}(x_w f)^2$ for the insects listed in Fig. 10A, where $\boldsymbol{g}$ is the acceleration due to gravity, S_{tot} is the total wing surface area of four wings of an insect, and x_w is the length of the forewing. The fluid-dynamic force generated by a wing is proportional to $S_{tot}(x_w f)^2$, where $x_w f$ is proportional to the mean velocity of the flow around the wing. Therefore, the parameter $m\boldsymbol{g}/S_{tot}(x_w f)^2$ reflects the coefficient of vertical fluid-dynamic force generated by an insect. For the thrips $m\boldsymbol{g}/S_{tot}(x_w f)^2 \approx 25$; this is larger than that for *Bemisia tabaci*, *Aleurothrixus floccosus*, *Aphis gossypii* and *Acyrthosiphon kondoi*, which have membranous wings. The larger value of $m\boldsymbol{g}/S_{tot}(x_w f)^2 \approx 25$ for thrips can be explained by the larger values of C_L and C_D for a bristled model wing compared with the coefficients for the solid model wing.

The resultant force of the lift and drag generated by the thrips was approximately 5×10^7 N at any flapping angle with the following assumptions: (i) the thrips has four wings whose size is shown in Table 1; (ii) the flapping motion is the same as defined for the accelerating rotation at *f*=200 Hz; and (iii) the geometrical angle of attack is 45°, and changes over time in the lift and drag coefficients are given by those of the bristled wing in Fig. 9A. The estimated value of the vector sum of lift and drag is close to the gravitational force acting on the thrips (6×10^7 N). However, to understand more fully the flight of the thrips, we need a more precise estimate of the fluid-dynamic forces generated by their wings, based on more accurate data on wing morphology and kinematics, on the variation in angle of attack (feathering angle), and lift and drag coefficients measured over several consecutive wing beats.

List of symbols

c	Chord length of a wing
c_m	Membrane width of a bristled wing
c_{h1}	Length of cylinders or bristles attached at the leading edge of the bristled wing
c_{h2}	Length of cylinders or bristles attached at the trailing edge of the bristled wing
C_L, C_D	Lift and drag coefficients, respectively
d	Diameter of cylinders or bristles
D	Distance between neighbouring cylinders or bristles
f	Wing-beat frequency
F_n, F_t	Normal and tangential forces, respectively
$F_{n,c}$, $F_{t,c}$	Normal and tangential forces, respectively, measured on the wing mount without a wing connected to it
F_Z, M_Z	Force in Z axis and moment around Z axis, respectively
F_x, F_z, M_y	Forces in x,z axes and moment around y axis, respectively
$\boldsymbol{g}$	Acceleration of gravity
L_X, L_Y, L_Z	Dimensions of the tank
L_{Z1}	Depth of liquid
m	Mass of an insect
m_w	Mass of a wing
n	The number of cylinders or bristles of a bristled wing
Q	Torque
Q_c	Torque measured in air
Re	Reynolds number
S	Wing surface area
S_{tot}	Total wing surface area of an insect
t	Time
t_m	Thickness of a wing
T	Thrust
T_{0r}	Period of accelerated phase in rotational motion
T_{0t}	Period of accelerated phase in translational motion
V_0	Terminal forward velocity
x, y, z	Wing-fixed coordinate system
x_w	Wing length
X, Y, Z	Earth-fixed coordinate system
α	Angle of attack
ν	Kinematic viscosity
ρ	Density of fluid
$\Phi/2$	Amplitude of accelerating rotational motion
Φ	Rotational angle
ω	Angular velocity for constant-velocity rotation

We would like to thank the anonymous referees for their critical and important comments on the manuscript. This research was financially supported by the Research and Development for Applied Advanced Computational Science and Technology of the Japan Science and Technology Corporation.

References

Azuma, A. (1992). *The Biokinetics of Flying and Swimming*. Tokyo: Springer-Verlag.

Cheer, A. Y. L. and Koehl, M. A. R. (1987). Paddles and rakes: fluid flow through bristled appendages of small organisms. *J. Theor. Biol.* **129**, 17–39.

Dickinson, M. H., Lehmann, F. and Sane, S. P. (1999). Wing rotation and the aerodynamic basis of insect flight. *Science* **284**, 1954–1960.

Ellington, C. P. (1980). Wing mechanics and take-off preparation of thrips (Thysanoptera). *J. Exp. Biol.* **85**, 129–136.

Ellington, C. P. (1984). The aerodynamics of hovering flight. II. Morphological parameters. *Phil. Trans. R. Soc. Lond. B* **305**, 17–40.

Hansen, B. and Tiselius, P. (1992). Flow through the feeding structures of suspension feeding zooplankton: a physical model approach. *J. Plankton Res.* **14**, 821–834.

Hoerner, S. F. (1965). *Fluid-dynamic Drag*. Midland Park, NJ: Published by the author.

Horridge, G. A. (1956). The flight of very small insects. *Nature* **178**, 1334–1335.

Koehl, M. A. R. (1983). The morphology and performance of suspension-feeding appendages. *J. Theor. Biol.* **105**, 1–11.

Koehl, M. A. R. (1995). Fluid flow through hair-bearing appendages: feeding, smelling and swimming at low and intermediate Reynolds numbers. In *Biological Fluids Dynamics* (ed. C. P. Ellington and T. J. Pedley). *Symp. Soc. Exp. Biol.* **49**, 157–182. Cambridge: Company of Biologists.

Kuethe, A. M. (1975). On the mechanics of flight of small insects. In *Swimming and Flying in Nature*, vol. 2 (ed. T. Y. T. Wu, C. J. Brokaw and C. Brennen), pp. 803–813. New York: Plenum.

Tanaka, S. (1995). Thrips' flight. Part 1. In *Symposia '95 of Exploratory Research for Advanced Technology, Japan Science and Technology Corporation*, Abstracts (ed. K. Kawachi), pp. 27–34. Tokyo: Japan Science and Technology Corporation (in Japanese).